scientific reports

Check for updates

OPEN

PARIS/ZNF746 DNA-binding domain deficiency promotes adipose tissue hyperplasia and hepatic lipid accumulation

Kazuki Hachiya[1], Yuhei Mizunoe[1], Joo-Joo Yang[1], Yuki Uchida[1], Hiroto Fukai[1], Tatsuhiro Esashi[1], Yuka Nozaki[1], Seiya Mizuno[4], Satoru Takahashi[4], Masaki Kobayashi[1,2,3] & Yoshikazu Higami[1,5]✉

Zinc finger protein 746 (ZNF746), also known as PARKIN-interacting substrate (PARIS), is a KRAB-ZFP family transcriptional repressor implicated in Parkinson's disease and adipogenesis. Its unclear role in systemic metabolism led us to investigate PARIS-mediated metabolic function by generating mice with a knockout of *Znf746* exon 7 (P7KO), containing the DNA-binding domain. Under a high-fat diet, P7KO mice exhibited larger gains in body and adipose tissue weight alongside improved insulin sensitivity and reduced adipocyte size compared with wild-type mice, suggesting hyperplastic expansion of white adipose tissue. P7KO mice also showed elevated anti-inflammatory markers in adipose tissues, in contrast to accumulation of lipids and upregulation of lipogenic genes, without changes in glucose transporter or lipid uptake genes, in the liver. These findings indicate a dual role for PARIS: suppressing adipose hyperplasia and restricting hepatic lipogenesis. Identification of the evolutionary conservation of PARIS among mammals, particularly the shared DNA-binding domain between mice and humans, support its translational relevance. Collectively, our results identify PARIS as a previously unrecognized regulator of metabolic homeostasis that coordinates lipid storage and utilization in a tissue-specific manner. Targeting PARIS may offer a novel therapeutic strategy for obesity-related metabolic disorders, such as type 2 diabetes and non-alcoholic fatty liver disease.

Diabetes is a growing global health concern, affecting approximately 537 million people in 2021, with nearly 90% classified as type 2 diabetes (T2D). This number is estimated to reach 783 million by 2045[1]. Obesity, a key risk factor for T2D, is highly prevalent among T2D patients, of whom > 80% are considered overweight or obese[2]. Sustained weight loss has been shown to reduce metabolic burden and delay progression from prediabetes to T2D[3]. Given the continuing rise in global obesity rates driven by modern lifestyle practices, there is an urgent need for fundamental research to develop effective therapeutic strategies[4].

The pathophysiology of T2D is characterized by insulin resistance and progressive beta cell dysfunction leading to hyperglycemia[5]. Once insulin-targeted tissues, such as white adipose tissue (WAT), liver, and skeletal muscle, become insulin resistant due to factors such as obesity, pancreatic beta cells respond by releasing excessive amounts of insulin. Excess insulin production leads to hyperinsulinemia and beta cell exhaustion, and the expansion of adipose tissue in response to excess energy intake may critically influence the development of insulin resistance. Adipose tissue expansion is classified into two types: one resulting from an increase in the size of adipocytes (hypertrophy), and the other from an increase in the number of adipocytes (hyperplasia)[6]. Numerous studies have suggested that these expansion types have distinct effects on whole-body metabolism[7–11], with hyperplastic adipose tissue being associated with relatively lower inflammation and higher insulin sensitivity compared with hypertrophic adipose tissue[12]. These findings suggest that regulation of the balance between hyperplasia and hypertrophy in adipose tissue expansion could be critical for metabolic homeostasis.

[1]Laboratory of Molecular Pathology and Metabolic Disease, Faculty of Pharmaceutical Sciences, Tokyo University of Science, Chiba, Japan. [2]Department of Nutrition and Food Science, Graduate School of Humanities and Sciences, Ochanomizu University, Tokyo, Japan. [3]Institute for Human Life Science, Ochanomizu University, Tokyo, Japan. [4]Laboratory Animal Resource Center and Trans-Border Medical Research Center, University of Tsukuba, 1-1-1 Tennodai, Tsukuba, Ibaraki 305-8575, Japan. [5]Research Institute for Biomedical Sciences (RIBS), Tokyo University of Science, Noda, Japan. ✉email: higami@rs.tus.ac.jp

Recently, two studies demonstrated the possibility that PARKIN-interacting substrate (PARIS), encoded by *Znf746* in mice, contributes to the development of T2D[13,14]. In one of these, we found that PARIS is highly expressed in adipose progenitor cells in WAT and that diet-induced obesity leads to further accumulation of PARIS in mice, resulting in impaired adipogenesis[13]. We also demonstrated that an abundance of PARIS in adipose progenitor cells inhibits their differentiation, acting as a gatekeeper of adipogenesis. Complementing these observations, recent in silico approaches highlighted PARIS as a potential contributor to T2D pathogenesis. A genome-wide association study (GWAS) identified PARIS (*ZNF746*) as a T2D-related gene[14], suggesting its potential relevance beyond animal models. These findings raise the possibility that PARIS plays a conserved role in metabolic regulation. However, the molecular mechanisms by which PARIS contributes to metabolic dysfunction remain largely unexplored, warranting further investigation into its cross-species roles and downstream pathways. Based on these observations, we hypothesized that PARIS contributes to metabolic dysfunction, and that its deficiency may lead to improved metabolic outcomes in mice fed with a high-fat diet (HFD).

This study aims to elucidate the role of PARIS in metabolic regulation, particularly under dietary stress conditions. To achieve this, we generated *Znf746* knockout (KO) mice and subjected them to a HFD to assess the impact of PARIS deficiency on systemic metabolism. While PARIS has been primarily studied in the context of neurodegenerative diseases[15–17], this study provides direct in vivo evidence of its function in metabolic homeostasis. Our findings advance the understanding of PARIS as a novel metabolic regulator and may offer insights into potential therapeutic targets for obesity-related disorders.

Results

ZNF746 single-nucleotide polymorphisms (SNPs) associated with metabolic traits in GWASs

To investigate potential associations between PARIS and metabolic traits, we used the GWAS Catalog, a comprehensive database that curates published GWAS data and provides detailed information on genetic variants associated with various traits and diseases[18]. Through this analysis, we identified nine GWASs that included *ZNF746* (Table 1). In addition to the previously reported association with T2D[14], *ZNF746* was found to be linked to several metabolic traits, including levels of apolipoprotein B, triglycerides, and blood pressure (Table 1).

Notably, these three traits are key risk factors for metabolic syndrome, which is closely associated with T2D. The identification of *ZNF746* as a shared genetic factor for multiple metabolic traits highlights its potential role as a regulator of systemic metabolic dysfunction. This finding also suggests that PARIS may contribute to the pathogenesis of T2D and related metabolic disorders by influencing lipid metabolism and cardiovascular health. Further investigation to elucidate the molecular mechanisms underlying these associations is warranted.

ZNF746 is highly conserved among mammals and suitable for functional studies in mice

Given the observed associations between *ZNF746* and metabolic traits in humans, we sought to further investigate its role using a mouse model. To establish the relevance of this model, we first evaluated the evolutionary conservation of *ZNF746* across different species.

According to the Ensembl database, *ZNF746* orthologs are present in 317 of 553 mammalian species, four of eight bird species, and seven of 19 reptile species, with no orthologs identified in 66 fish species[19] (Fig. 1A). The distribution pattern of *ZNF746* orthologs indicates that its presence is primarily restricted to terrestrial vertebrates. Further analysis of the Ensembl gene tree for human *ZNF746* revealed that its evolutionary distance between primates and rodents is relatively short, suggesting a close evolutionary relationship in these species (Fig. 1B)[19].

Because PARIS is thought to function as a DNA-binding transcription factor, we performed a sequence alignment of the putative nucleic acid-binding domains of the human and mouse genes to assess the validity of a functional comparison between these species. The alignment revealed that the two sequences were completely identical (Fig. 1C). Based on these findings, we considered the function of PARIS to be highly conserved between humans (NP_001156946.1) and mice (NP_001156947.1). Therefore, we generated *Znf746* KO mice to further elucidate the role of PARIS in metabolic regulation.

riskAllele	p value	Mapped genes	Trait name	Accession ID
rs6972751-?	2.00E-06	ZNF746	General cognitive ability	GCST006269
rs150290553-A	9.00E-06	ZNF746	Apolipoprotein B levels (adjusted for BMI) x vegetarianism interaction	GCST90161208
rs6949316-?	4.00E-08	ZNF746	Triglyceride levels	GCST90239661
rs6972751-T	2.00E-09	ZNF746	Type 2 diabetes	GCST90492734
rs11974139-C	5.00E-11	ZNF746,ZNF777	Monocyte count	GCST90002340
rs855913-A	4.00E-08	ZNF746,ZNF767P	Amyotrophic lateral sclerosis	GCST000406
rs115476423-?	5.00E-06	ZNF746,ZNF767P	Blood pressure traits (multi-trait analysis)	GCST004388
rs62490267-C	5.00E-08	ZNF746,ZNF767P	Type 2 diabetes	GCST010557
rs855917-G	3.00E-08	ZNF767P,ZNF746	Cerebral aneurysm	GCST90013762
rs144738335-T	2.00E-06	ZNF777,ZNF746	Time to colon cancer recurrence	GCST90060090

Table 1. SNPs associated with metabolic and non-metabolic traits in or near *ZNF746* identified through GWAS studies. Data derived from the GWAS Catalog (https://www.ebi.ac.uk/gwas/), accessed March 20, 2025.

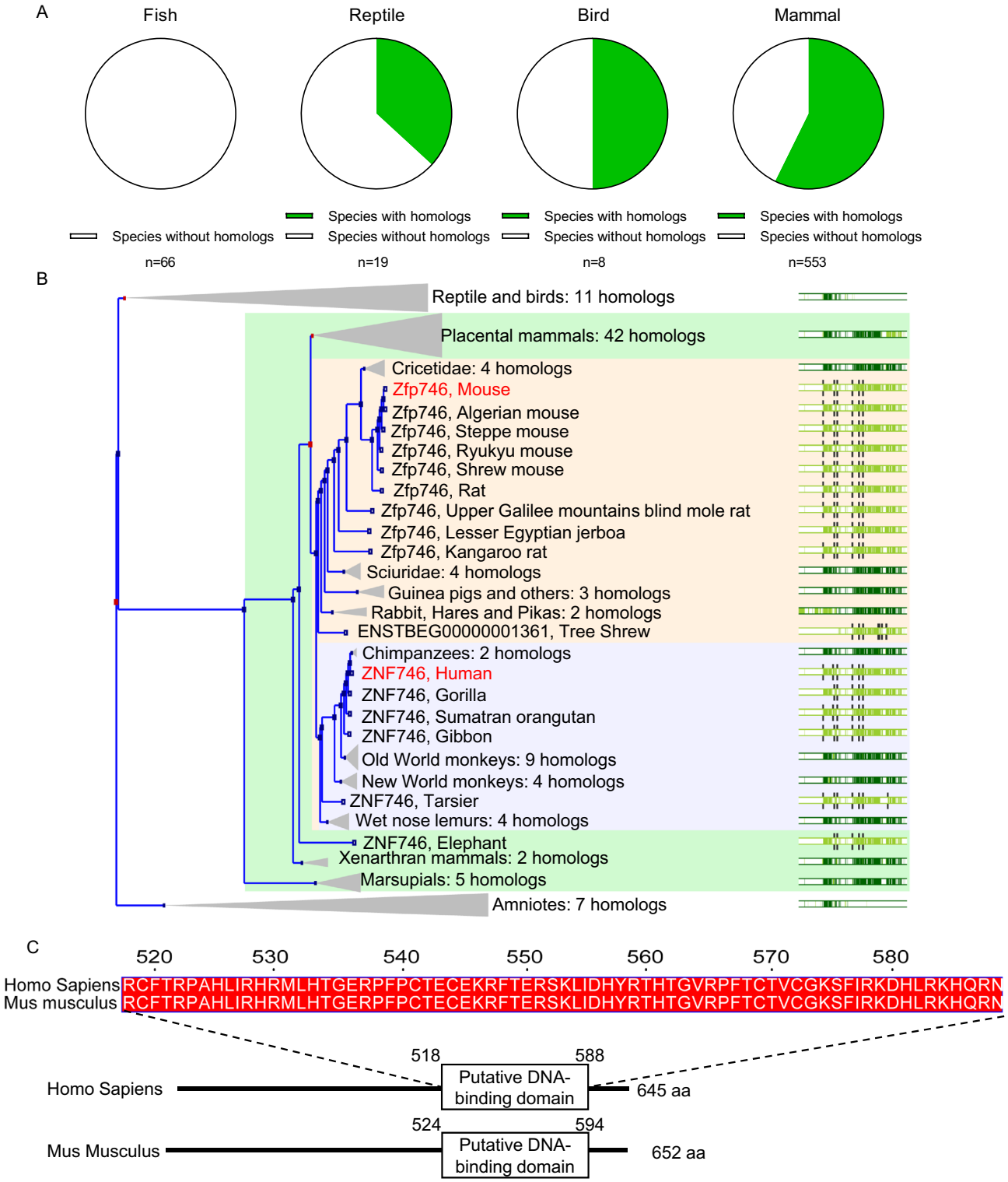

Fig. 1. Analysis of PARIS (*ZNF746*) orthologs in vertebrates. (**A**) Phylogenetic distribution of *ZNF746* orthologs across vertebrates based on the Ensembl database [19]. Pie charts represent the proportion of species with (green) and without (white) *ZNF746* orthologs in each vertebrate group. (**B**) Phylogenetic tree of *ZNF746* orthologs based on the Ensembl gene tree [19]. Primates and rodents are highlighted with blue and orange backgrounds, respectively. (**C**) Sequence alignment showing the amino acid sequence of the putative DNA-binding domain of PARIS in humans and mice.

Generation of KO mice with targeted deletion of the PARIS DNA-binding domain

To investigate the function of PARIS, we generated PARIS knockout mice (P7KO) lacking the exon 7 of the *Znf746*, which contains its putative DNA-binding site. The deletion of exon 7 and the subsequent loss of PARIS were validated at the mRNA level in subcutaneous (s)WAT and epididymal (e)WAT (Supplementary Fig. S1F).

Next, we tested the protein expression of PARIS in P7KO mice using western blotting. Polyclonal antibodies against PARIS successfully distinguished wild type (WT) from P7KO samples, validated the KO of the protein in several tissues (Supplementary Fig. S2A, B). However, the monoclonal antibody exhibited some non-specific binding in P7KO mice (Supplementary Fig. S2A, C). Because both antibodies were generated using human PARIS as an immunogen, their specificity for mouse PARIS remains uncertain. It should be noted that Entrop and colleagues recently reported that even widely used antibodies sometimes lack specificity for their target proteins[20]. Notably, in non-WATs, the polyclonal antibodies detected PARIS at a slightly lower molecular weight compared with that in WATs, suggesting the presence of a smaller PARIS variant in these tissues. Therefore, the polyclonal anti-PARIS antibody was used for all subsequent experiments.

PARIS KO mice show exaggerated adipose expansion under HFD

Building on our previous finding of PARIS-mediated inhibition of adipocyte differentiation and confirmation of the anti-PARIS antibody selectivity, we examined P7KO and WT mice for body and adipose tissue weight. Under normal diet (ND) conditions, P7KO and WT mice showed no significant differences in total body weight or in the weights of sWAT, eWAT, kidney, liver, lung, or heart (Fig. 2A,B). To examine the role of PARIS under dietary stress, the mice were fed a HFD (Fig. 2C) and assessed for metabolic phenotype. P7KO mice on a HFD exhibited significantly greater body weight gain than WT mice (Fig. 2D, E), despite no significant difference in food intake (Fig. 2F). Computed tomography (CT) analysis further revealed that adipose tissue expansion was more pronounced in P7KO mice than in WT mice under HFD conditions (Fig. 2G). Weight measurements revealed that sWAT and livers were significantly larger in P7KO mice than in WT mice (Fig. 2H, I), with no significant differences in other individual adipose tissues or organs. Notably, macroscopic examination showed that P7KO liver tissue was paler in color than WT liver tissue (Fig. 2H).

PARIS deficiency improves insulin sensitivity under HFD

To evaluate the effect of PARIS deficiency on glucose metabolism, we performed intraperitoneal glucose tolerance tests (GTTs) and insulin tolerance tests (ITTs) in HFD-fed WT and P7KO mice (Fig. 3). The GTT results showed a trend toward lower blood glucose levels in P7KO mice compared with that in WT mice (Fig. 3A), with area under the curve (AUC) analysis approaching statistical significance ($P = 0.08$, Fig. 3B). Consistently, the ITT results demonstrated an improvement in insulin sensitivity in P7KO mice. Post insulin injection, blood glucose levels were significantly lower in P7KO mice than in WT mice (Fig. 3C). This enhancement in insulin sensitivity was confirmed by the AUC analysis (Fig. 3D).

PARIS deficiency leads to smaller adipocytes in eWAT

Given the prominent increases in sWAT and liver weight, but not eWAT weight, in P7KO mice, we conducted a detailed analysis of eWAT, sWAT, and liver tissues. First, we measured PARIS protein levels in eWAT of WT and P7KO mice fed either ND or HFD using the validated polyclonal antibody (Fig. 4A,B). Consistent with our previous report[13], PARIS protein levels were elevated in eWAT of WT mice under HFD conditions (Fig. 4A,B).

Considering that P7KO mice exhibited greater increases in body and sWAT weights (Fig. 2D,E,G–I) along with improved insulin sensitivity compared with WT mice (Fig. 3A–D) under HFD, we hypothesized that these changes might reflect hyperplastic adipose tissue expansion. Because a decrease in adipocyte size is considered to indicate an increase in adipocyte number rather than hypertrophy, we tested this hypothesis by examining adipocyte size in eWAT using hematoxylin and eosin (H&E)-stained sections (Fig. 4C,D; Supplementary Fig. S3A, B). Indeed, we found that adipocytes in P7KO mice were smaller in size than those in WT mice, regardless of the diet.

To assess inflammation, we measured mRNA levels of interleukins IL-6 (*Il6*) and IL-10 (*Il10*) using RT-PCR. While *Il6* expression remained unchanged, that of *Il10*, an anti-inflammatory cytokine, was increased in eWAT of HFD-fed P7KO mice (Fig. 4E).

Under ND conditions, P7KO mice exhibited reduced mRNA levels of peroxisome proliferator-activated receptor (PPAR)γ1 and PPARγ2 in eWAT compared with WT mice (Supplementary Fig. S3G), while the relative protein levels of the two isoforms remained unchanged (Supplementary Fig. S3E, F). In contrast, under HFD conditions, the protein level of PPARγ2, a key regulator of adipocyte differentiation, was markedly decreased relative to PPARγ1 in eWAT of P7KO mice (Fig. 4F,G), with a similar trend in mRNA expression (Fig. 4H). Consistently, the expression levels of several PPARγ downstream genes (*Adipoq*, *Fasn*, *Acaca*, and *Srebf1*) were also decreased in eWAT under HFD conditions (Fig. 4H). Notably, the expression levels of these downstream genes showed reductions even under ND conditions in P7KO mice (Supplementary Fig. S3G). Furthermore, despite the reduction in PPARγ2 protein levels, the mRNA expression of *Cebpa*, another key regulator of adipogenesis, was maintained in eWAT of P7KO mice (Fig. 4H). The expression level of *Ppargc1a*, a known direct target of PARIS[16], in eWAT of P7KO mice did not differ from that in WT mice, regardless of the diet (Fig. 4H; Supplementary Fig. S3G).

PARIS deficiency leads to hyperplastic sWAT expansion under HFD

Next, we analyzed sWAT, which showed the most pronounced increase in weight among the examined tissues. In contrast to eWAT, PARIS protein levels in sWAT were not affected by HFD feeding in WT mice (Fig. 5A,B). Similar to eWAT, adipocytes in P7KO mice were smaller than those in WT mice under both ND and HFD

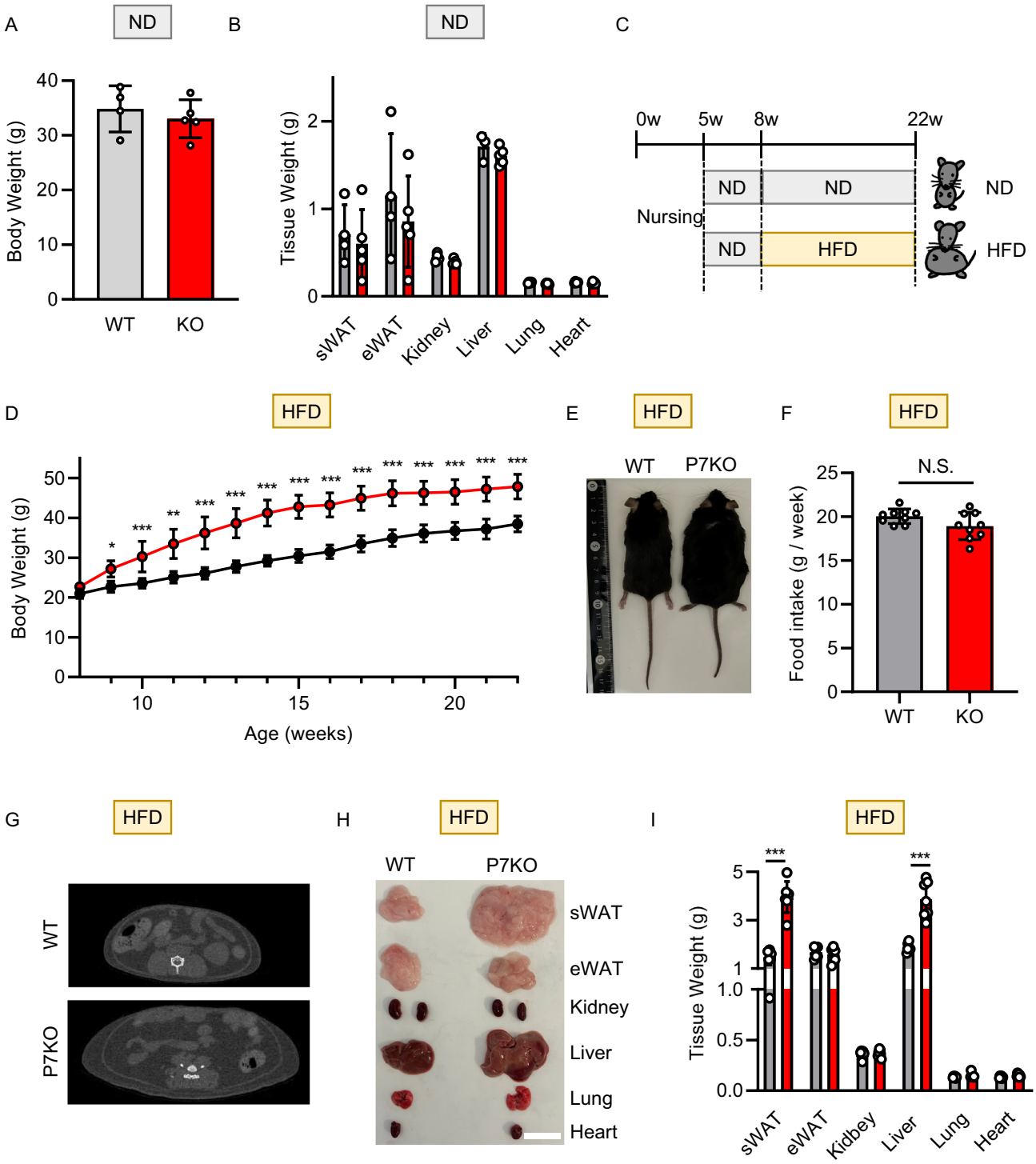

Fig. 2. Overview of the P7KO mouse phenotype under HFD conditions. (**A**,**B**) Total body (**A**) and tissue (**B**) weights of WT and P7KO mice at 22 weeks of age under ND (n = 4–5). (**C**) Feeding schedule for ND control and HFD modeling. (**D**) Body weight of WT and P7KO mice under HFD over time (n = 6–7). (**E**) Representative photograph of HFD-fed WT (left) and P7KO (right) mice. (**F**) Weekly food intake of HFD-fed WT and P7KO mice (n = 9). (**G**) Representative CT images of HFD-fed WT (top) and P7KO (bottom) mice at 16 weeks of age. (**H**) Representative photograph and (I) weights of individual tissues and organs collected from HFD-fed WT and P7KO mice (n = 6–7). Scale bar: 2 cm. Data expressed as means ± standard deviation (SD), analyzed by Student's t-test; *P < 0.05, **P < 0.01, ***P < 0.001.

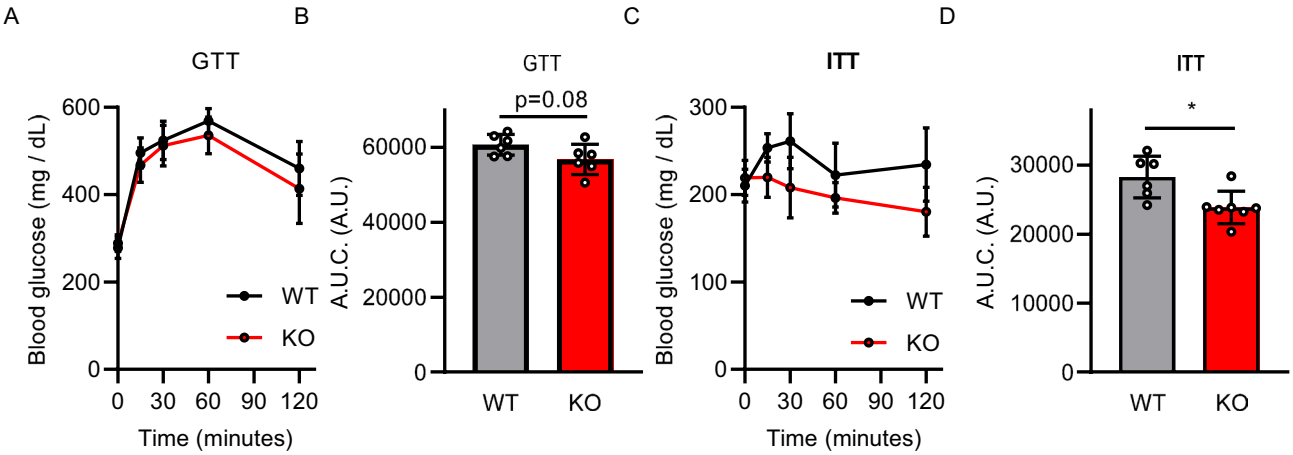

Fig. 3. Analysis of whole-body glucose metabolism in HFD-fed WT and P7KO mice. (**A**,**B**) GTT curve (**A**) of WT and P7KO mice at 20 weeks of age (n = 6–7), with corresponding quantitative analysis illustrated as AUC (B). (**C**,**D**) ITT curve of WT and P7KO mice at 19 weeks of age (n = 6–7), with corresponding quantitative analysis illustrated as AUC (**D**). Data expressed as means ± SD, analyzed by Student's t-test; *P < 0.05, **P < 0.01, ***P < 0.001.

(Fig. 5C,D; Supplementary Fig. S3C, D). While *Il6* mRNA expression did not differ between the P7KO and WT groups, *Il10* expression was increased in P7KO mice under HFD (P = 0.057) (Fig. 5E).

Under ND conditions, the protein levels of both PPARγ1 and PPARγ2 in sWAT did not differ between P7KO mice and WT controls (Supplementary Fig. S3E, F), with similar trends in mRNA expression (Supplementary Fig. S3G). Expression of PPARγ downstream genes (*Adipoq*, *Fasn*, *Acaca*, and *Srebf1*) was preserved and, although not statistically significant, *Cebpa* expression was increased in the P7KO group. *Ppargc1a* expression did not differ between the groups (Supplementary Fig. S3G).

Under HFD conditions, the protein levels of PPARγ2 relative to PPARγ1 were significantly reduced in sWAT of P7KO mice (Fig. 5F,G), despite the lack of any significant change in the mRNA expression of either *Pparg* isoform (Fig. 5H). The reduction in PPARγ2 protein did not impact the expression levels of PPARγ downstream genes (*Adipoq*, *Fasn*, *Acaca*, and *Srebf1*), which were preserved (Fig. 5H). Furthermore, while *Cebpa* expression was upregulated in P7KO mice (Fig. 5H), *Ppargc1a* expression remained unchanged, consistent with the findings in eWAT (Fig. 5H).

PARIS deficiency leads to hepatic lipid accumulation

Considering the significant liver enlargement observed in P7KO mice fed a HFD (Fig. 2H,I), we sought to compare PARIS protein levels in the liver between ND and HFD conditions (Fig. 6A). WT mice fed a HFD showed elevated PARIS levels compared with those fed a ND (Fig. 6B). To further explore the impact of PARIS deficiency on liver function under HFD conditions, we conducted a comprehensive analysis of hepatic metabolism in P7KO mice.

Although no histological differences in H&E-stained liver sections were observed between the groups under ND conditions (Supplementary Fig. S4A), this staining revealed greater numbers of lipid vacuoles in P7KO hepatocytes than in WT hepatocytes under HFD conditions (Fig. 6C), consistent with the paler appearance of the liver in HFD-fed P7KO mice (Fig. 2H). Furthermore, biochemical analysis demonstrated significantly higher levels of triglycerides (Fig. 6D) and total cholesterol (Fig. 6E) in the liver of P7KO mice, confirming the increase in hepatic lipid accumulation.

In contrast to WAT, where PPARγ2 expression was selectively reduced under HFD conditions in P7KO mice, the liver, which expresses only the PPARγ1 isoform, exhibited comparable PPARγ1 protein levels between the groups under both ND and HFD conditions (Fig. 6F,G; Supplementary Fig. S4B, C). Expression levels of genes involved in lipid uptake (*Cd36*) and glucose uptake (*Slc2a2*, encoding GLUT2) showed no significant differences between WT and P7KO mice under ND conditions (Supplementary Fig. S4D), with similar results observed under HFD conditions (Fig. 6H). By contrast, genes encoding major regulators of lipid metabolism, including the transcription factor SREBP-1c (*Srebf1*), fatty acid synthase (*Fasn*), and ATP citrate lyase (*Acly*), were significantly upregulated in the liver of P7KO mice under both ND and HFD conditions (Fig. 6H; Supplementary Fig. S4D).

Consistent with findings in WAT, the liver expression of *Ppargc1a* did not differ between P7KO mice and WT controls under either diet (Fig. 6H; Supplementary Fig. S4D).

Discussion

In this study, we demonstrated that, despite greater increases in body, adipose tissue, and liver weight under HFD, PARIS-deficient mice exhibited favorable glucose metabolism compared with WT mice. By contrast, the impact of PARIS deficiency under ND conditions was relatively minor. These findings suggest that PARIS, initially identified as a pathogenic molecule involved in Parkinson's disease (PD)[16], plays a crucial role in the metabolic response to dietary stress. In PD models, PARIS accumulation due to Parkin deficiency leads to mitochondrial

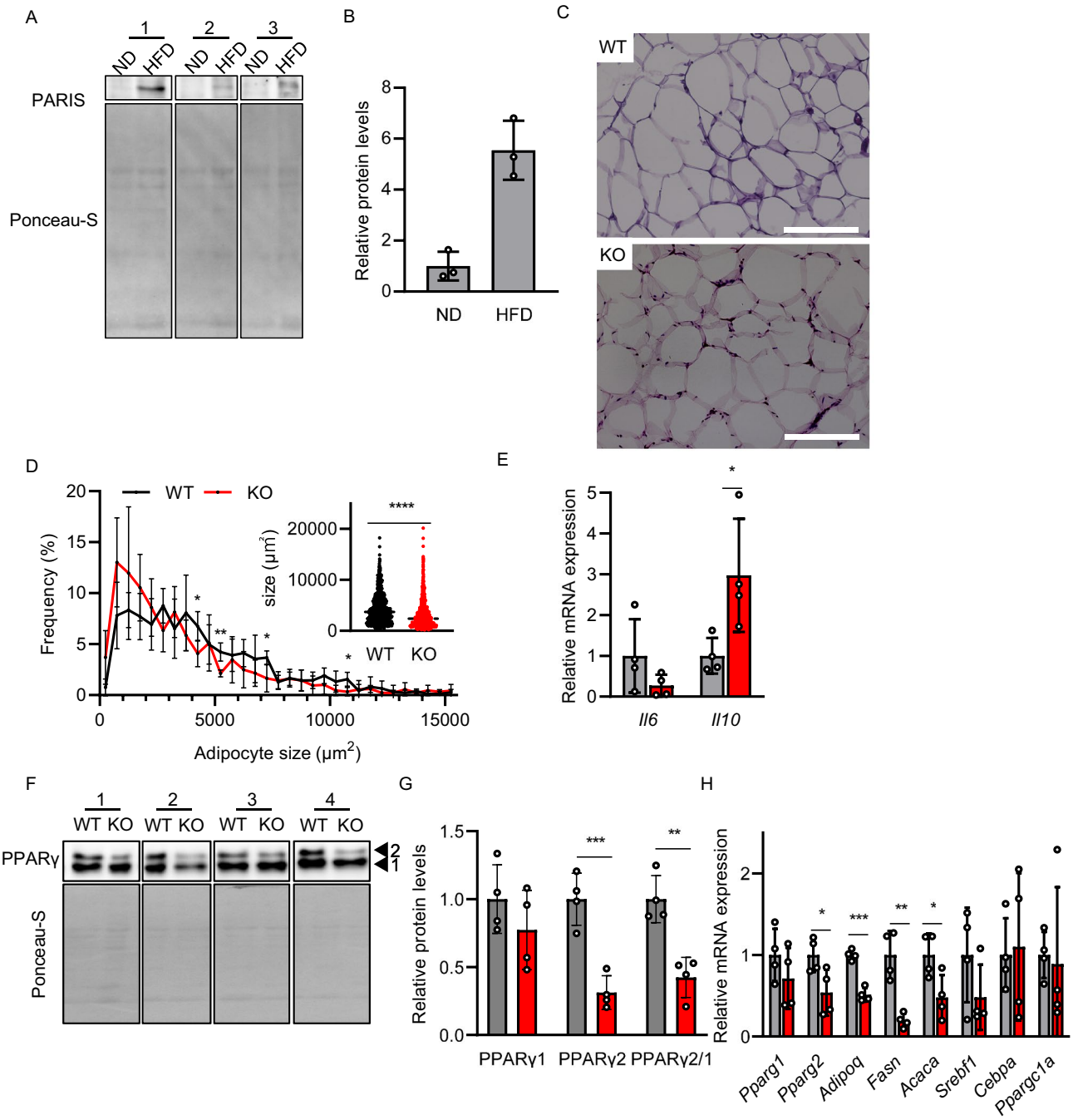

Fig. 4. Analysis of eWAT in HFD-fed WT and P7KO mice. (**A**) Western blotting and (**B**) quantitative analysis of PARIS expression in eWAT of WT (W; gray bars) mice fed with ND or HFD. Data presented as means ± SD, analyzed by two-way analysis of variance (ANOVA) followed by Tukey's multiple comparisons test; ****P < 0.0001. (**C**) Representative microscopic images of H&E-stained eWAT of WT and P7KO (KO) mice. Scale bars: 200 μm. (**D**) Distribution curve and box plot of adipocyte size in the two groups: WT, n = 814 cells from four mice; KO, n = 1,143 cells from four mice. (**E**) RT-PCR analysis of mRNA expression of *Il6* and *Il10* in eWAT of WT (gray bars) and P7KO (red bars) mice. (**F**) Western blotting and (**G**) quantitative analysis of PPARγ isoforms 1 and 2 in eWAT of WT and P7KO mice (n = 4). Ponceau-S staining was used for normalization. (**H**) RT-PCR analysis of mRNA expression of *Pparg1*, *Pparg2, Adipoq*, *Fasn*, *Acaca*, *Srebf1*, *Cebpa*, and *Ppargc1a* in eWAT of WT and P7KO mice. Data expressed as means ± SD, analyzed by Student's t-test; *P < 0.05, **P < 0.01, ***P < 0.001.

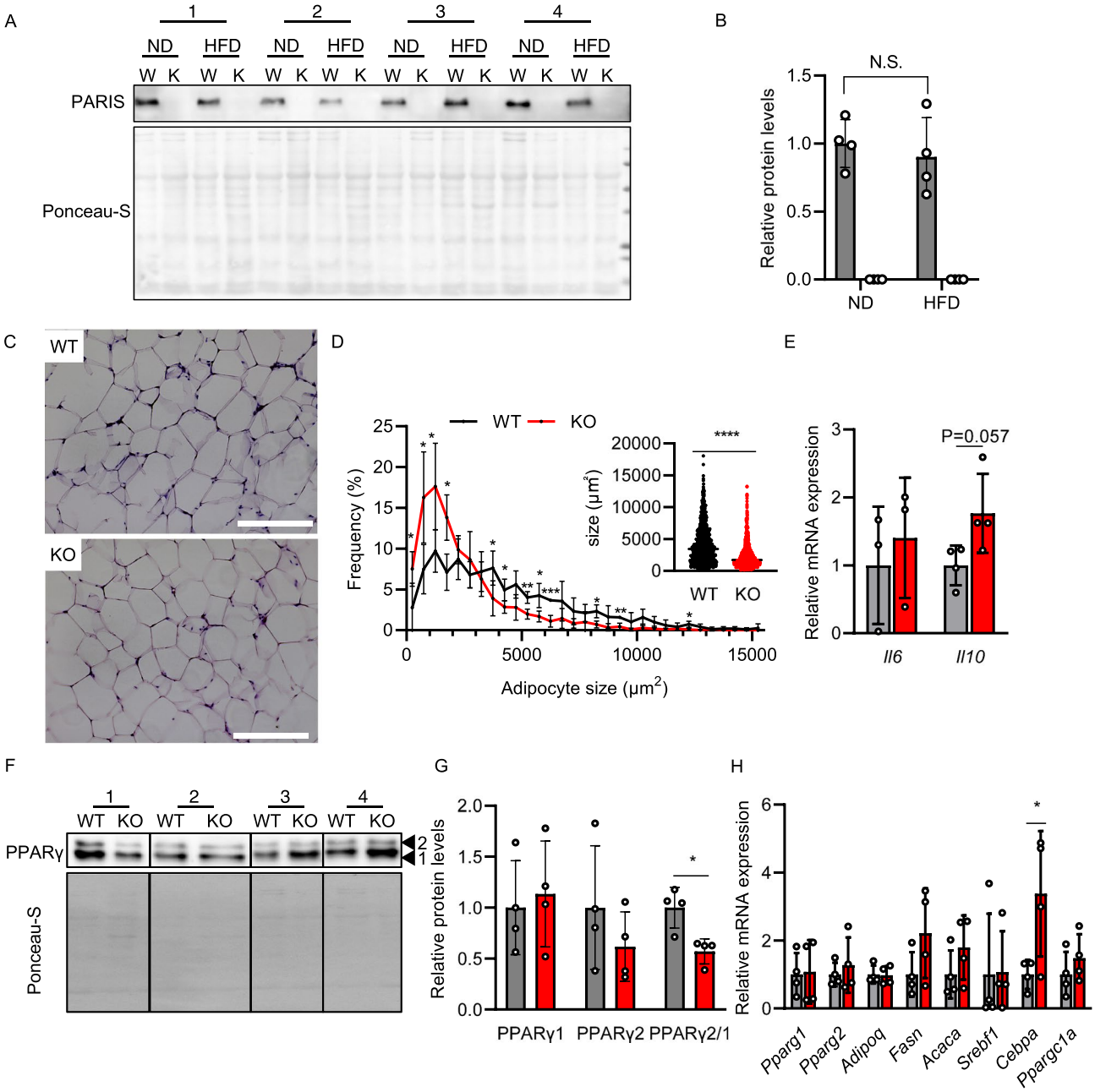

Fig. 5. Analysis of sWAT in HFD-fed WT and P7KO mice. (**A**) Western blotting and (**B**) quantitative analysis of PARIS expression in sWAT of WT (W; gray bars) and P7KO (K; undetectable) mice fed with ND or HFD. Data presented as means ± SD, analyzed by ANOVA followed by Tukey's multiple comparisons test. N.S. = not significant. (**C**) Representative microscopic images of H&E-stained sWAT of WT and P7KO (KO) mice. Scale bars: 200 μm. (**D**) Distribution curve and box plot of adipocyte size in the two groups: WT, n = 955 cells from four mice; KO, n = 1,743 cells from four mice. (**E**) RT-PCR analysis of mRNA expression of *Il6* and *Il10* in sWAT of WT (gray bars) and P7KO (red bars) mice. (**F**) Western blotting and (**G**) quantitative analysis of PPARγ isoforms 1 and 2 in sWAT of WT and P7KO mice (n = 4). Ponceau-S staining was used for normalization. (**H**) RT-PCR analysis of mRNA expression of *Pparg1*, *Pparg2, Adipoq*, *Fasn*, *Acaca*, *Srebf1*, *Cebpa*, and *Ppargc1a* in eWAT of WT and P7KO mice. Data expressed as means ± SD, analyzed by Student's t-test; *P < 0.05, **P < 0.01, ***P < 0.001.

dysfunction and neurodegeneration through the suppression of *PPARGC1a*, which encodes PGC-1α, a master regulator of mitochondrial biogenesis and metabolism[16,21]. Furthermore, a recent GWAS-based in silico analysis by Rabby and colleagues identified PARIS-encoding *ZNF746* as a T2D-related gene[14]. Moreover, our own analysis of the GWAS Catalog[18] has revealed that SNPs in or near the *ZNF746* locus are associated with key metabolic traits, including T2D and levels of triglycerides, apolipoprotein B, and blood pressure. PARIS was also previously shown to repress nuclear factor E2-related factor 2 (NRF2)-mediated transcription of genes

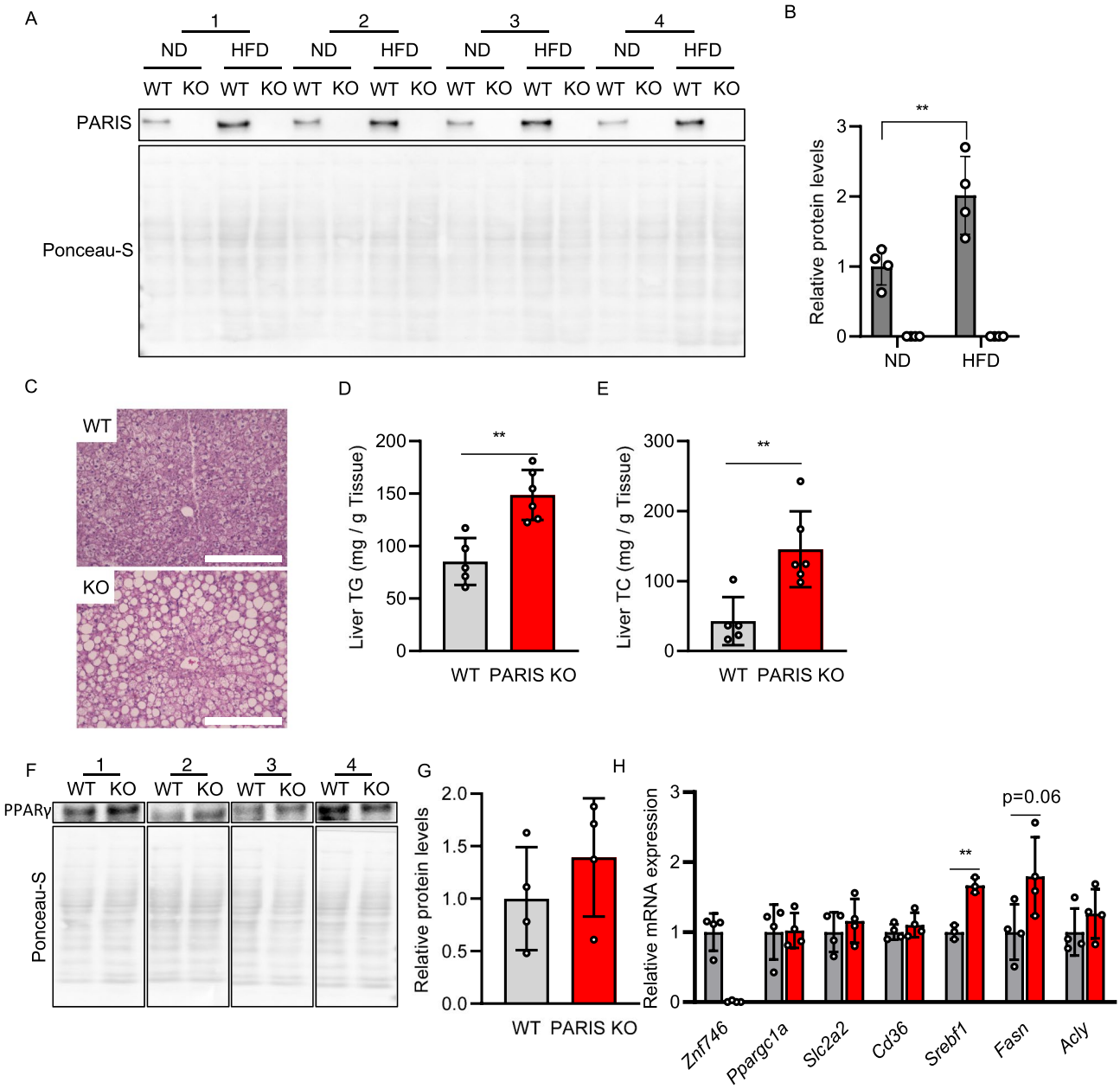

Fig. 6. Liver analysis of HFD-fed WT and P7KO mice. (**A**) Western blotting and (**B**) quantitative analysis of PARIS expression in the liver of WT (gray bars) and P7KO mice (KO; undetectable) fed with ND or HFD (n = 4). Ponceau-S staining was used for normalization. Data presented as means ± SD, analyzed by two-way ANOVA followed by Tukey's multiple comparisons test; **P < 0.01. (**C**) Representative microscopic images of H&E-stained liver sections of HFD-fed WT and P7KO mice. Scale bars: 200 µm. (**D**,**E**) Hepatic triglyceride (TG) and total cholesterol (TC) content in HFD-fed WT and P7KO mice (n = 5–6). (F, G) Western blotting (**F**) and quantitative analysis (**G**) of PPARγ expression in the liver of HFD-fed WT and P7KO mice (n = 4). Ponceau-S staining was used for normalization. Data presented as means ± SD. (H) RT-PCR analysis of mRNA expression of *Znf746*, *Ppargc1a*, *Slc2a2*, *Cd36*, *Srebf1*, *Fasn*, and *Acly* in the liver of HFD-fed WT and P7KO mice (n = 4). Data expressed as means ± SD, analyzed by Student's t-test; *P < 0.05, **P < 0.01, ***P < 0.001.

involved in redox homeostasis[17]. Taken together, these findings position PARIS as a key regulatory molecule at the intersection of mitochondrial function, redox balance, and systemic metabolism, implicating its involvement in the development of metabolic diseases such as T2D.

Here, in both sWAT and eWAT of HFD-fed P7KO mice, we observed smaller adipocytes, suppressed inflammation, and improved glucose metabolism compared with WT controls. These findings suggest that PARIS deficiency leads to hyperplastic WAT expansion. In our previous reports, we demonstrated that excessive PARIS inhibits adipogenesis through suppression of PPARγ signaling[13]. Supporting this, Yazar and colleagues employed a transgenic *Drosophila* model expressing human PARIS to demonstrate that PPARγ plays a central

role in the molecular alteration of neurons induced by PARIS. Furthermore, they demonstrated that PARIS directly binds to and suppresses the expression of PPARγ target genes[15]. Taken together, these findings suggest that PARIS contributes to the suppression of adipogenesis by directly repressing the expression of PPARγ target genes. Conversely, we observed that the protein level of PPARγ2, a master regulator of adipogenesis, was decreased in both sWAT and eWAT of P7KO mice compared with that in WT mice under HFD. Although the underlying mechanism remains unclear, this observation raises the possibility that PARIS may suppress negative regulators of PPARγ. Indeed, PARIS has been reported to directly repress transforming growth factor-β signaling, which inhibits PPARγ expression[15,22]. In addition, the observed discrepancy between mRNA and protein levels of PPARγ2 suggests the involvement of post-transcriptional regulatory mechanisms, such as microRNAs. Collectively, these findings indicate that additional layers of regulation beyond transcriptional control may contribute to the observed phenotype, warranting further investigation.

Although obesity is commonly associated with insulin resistance, the mechanism of adipose tissue expansion—hypertrophy versus hyperplasia—plays a crucial role in determining metabolic outcomes[6–11]. Several studies have demonstrated that hyperplastic expansion, characterized by an increased number of smaller adipocytes, is metabolically healthier than hypertrophic expansion, which involves fewer but larger adipocytes and is often accompanied by local inflammation and insulin resistance[6–11]. In our study, PARIS-deficient mice exhibited hyperplastic features in both sWAT and eWAT under HFD, including reduced adipocyte size and increased *Il10* expression, indicative of an anti-inflammatory environment. These changes were accompanied by improved systemic insulin sensitivity, as demonstrated by ITTs. Thus, our findings support the notion that promoting hyperplasia in adipose tissue may attenuate obesity-induced insulin resistance, potentially by preserving insulin-responsive adipocyte function and reducing proinflammatory signaling.

Consistent with our previous report, in which HFD feeding led to an increase in PARIS protein levels in eWAT[13], the current study also confirmed this HFD-induced increase in eWAT. In contrast, no such increase was observed in sWAT, which was analyzed for the first time in the current study. Several studies suggest that, under dietary stress, eWAT is more prone to inflammation, harbors more immune cells, and secretes greater amounts of inflammatory cytokines compared with sWAT[23–25]. Such differences in the microenvironment surrounding adipose progenitor cells may contribute to depot-specific accumulation of PARIS. Further investigation is needed to elucidate the mechanisms underlying this differential regulation.

Under HFD conditions, PARIS-deficient mice exhibited marked hyperplastic expansion of sWAT, characterized by preservation of PPARγ downstream signaling and upregulation of *Cebpa*, a key regulator of adipocyte differentiation. In contrast, although eWAT in PARIS-deficient mice showed some features of hyperplasia, such as reduced adipocyte size and lower inflammation, PPARγ downstream signaling was diminished. Compared with eWAT, sWAT is more prone to hyperplastic expansion[25,26]. Although many previous studies, including our own, have shown that excessive accumulation of PARIS suppresses *Ppargc1a* expression[13,16,21], we did not observe a significant increase in *Ppargc1a* expression in PARIS-deficient mice. This finding suggests that PARIS may not be the sole negative regulator of PGC-1α, and that other transcriptional repressors may compensate for its loss. For example, a review by Kobayashi and colleagues covering several pathways that negatively regulate PGC-1α expression[27] supports the plausibility that such compensatory mechanisms attenuate the impact of PARIS deficiency on PGC-1α levels. Therefore, the absence of *Ppargc1a* upregulation may reflect the presence of redundant regulatory networks, indicating that PARIS has additional functions beyond PGC-1α repression. Furthermore, despite the morphological features indicating enhanced adipogenesis in PARIS-deficient mice, we did not observe consistent increases in the mRNA expression of canonical adipocyte differentiation markers, such as *Pparg* and *Adipoq*. Jang and colleagues reported a similar finding in adipose-derived stem cells (ADSCs) derived from *Tc1* (*C8orf4*)-deficient mice, in which PPARγ expression was not significantly increased under basal conditions but was rapidly induced upon adipogenic stimulation in vitro[28]. These observations suggest that key transcriptional changes that occur only transiently during the early phase of adipocyte differentiation could be missed in whole-tissue analyses. Detailed in vitro studies using ADSCs from PARIS-deficient mice will be necessary to capture these dynamics and clarify the molecular mechanisms underlying hyperplastic expansion. In the meantime, it is plausible that PARIS deficiency does not directly promote hyperplasia, but instead removes a suppressive barrier, allowing the inherently hyperplasia-prone sWAT to expand more readily under HFD. Supporting this idea, a study involving *Tc1*-deficient mice found that enhanced adipocyte differentiation was accompanied by prominent hyperplastic expansion in sWAT[28]. Taken together, these findings support a model in which enhanced differentiation of adipose progenitor cells—unleashed by the loss of PARIS-mediated repression—leads to a more pronounced hyperplastic expansion in sWAT than in eWAT, likely reflecting the intrinsic depot-specific propensity of sWAT to undergo hyperplasia.

Notably, despite the increased adiposity in P7KO mice under HFD, insulin sensitivity was improved, suggesting depot-specific differences in insulin responsiveness. WAT, particularly sWAT, showed hyperplastic remodeling with preserved expression of PPARγ downstream genes and anti-inflammatory markers, consistent with an insulin-sensitive phenotype. In contrast, the liver of P7KO mice exhibited increased lipid accumulation and upregulation of lipogenic genes, despite no significant changes in the expression of glucose transporter (*Slc2a2*) or lipid uptake (*Cd36*) genes. These findings suggest that, while PARIS deficiency promotes insulin-sensitizing remodeling in adipose tissue, it may predispose the liver to lipogenesis without impairing its insulin responsiveness. This tissue-specific divergence highlights the complexity of systemic insulin sensitivity and underscores the importance of organ-specific regulation in metabolic homeostasis.

In the liver, we found that PARIS expression increased with obesity. Notably, in P7KO mice, hepatic expression of lipid uptake (*Cd36*) and glucose transporter (*Slc2a2*) genes remained unchanged, whereas key lipogenic genes such as *Srebf1* and *Fasn* were significantly upregulated, even under ND conditions. Furthermore, hepatic lipid accumulation was exacerbated in P7KO mice under dietary stress. These findings suggest that PARIS plays a role in suppressing hepatic lipogenesis, particularly in response to nutritional overload. This idea

is further supported by findings in *Drosophila* neurons, where human PARIS directly repressed genes involved in fatty acid metabolism[15]. Importantly, hepatic PPARγ levels were not altered in our P7KO mice, suggesting that PARIS may regulate hepatic lipid metabolism via PPARγ-independent mechanisms. Given that excessive hepatic lipid accumulation is a hallmark of non-alcoholic fatty liver disease (NAFLD), our data raise the possibility that PARIS protects against NAFLD by limiting hepatic lipogenesis under conditions of overnutrition.

Although we observed marked changes in the adipose tissue and liver of P7KO mice, we cannot exclude the possibility that these alterations are secondary to shifts in systemic energy balance, including central regulation by the brain. Further studies will be necessary to determine whether these phenotypes stem from direct effects of *Znf746* deficiency in each tissue or arise from systemic changes.

Collectively, our findings suggest that PARIS suppresses the expression of lipid metabolism genes in a tissue-specific manner: in WAT, where lipid storage is a primary function, this suppression limits fat accumulation; in the liver, a non-adipose organ, it plays a protective role by preventing ectopic lipid deposition.

The KRAB-ZFP gene family, to which PARIS belongs, is thought to have emerged over 400 million years ago in the common ancestor of coelacanths, lungfish, and tetrapods[29], undergoing rapid expansion in tetrapods through gene duplication[30]. The encoded proteins exhibit unusually high sequence homology compared with other transcription factor families[31–33]. In line with this, our comparative genomic analysis indicated that PARIS orthologs are widely distributed among mammals and other terrestrial vertebrates, but absent in fish. Sequence alignment further demonstrated complete identity in the DNA-binding domain between mouse and human PARIS, supporting the use of mouse models to study its function in metabolic regulation.

Nevertheless, the high degree of sequence similarity among KRAB-ZFPs presents technical challenges for experimental validation. While PARIS was detected predominantly in WAT in our previous study, broader expression was observed in the present study, including the kidneys, liver, and heart. This discrepancy may be attributable to specificity differences in the polyclonal and monoclonal antibodies that were employed, which recognize distinct epitopes. Given the extensive homology among KRAB-ZFP family members, rigorous validation of antibody specificity is crucial when interpreting protein expression data. Future studies employing genetic reporter systems or in situ hybridization will be essential to accurately determine the precise tissue distribution of PARIS.

Conclusion

This study identifies PARIS as a previously unrecognized regulator of peripheral metabolic homeostasis. In adipose tissue, PARIS suppresses hyperplastic expansion, while in the liver, it limits lipogenesis in response to dietary overload. The duality of these functions underscores the importance of PARIS in balancing systemic lipid storage and utilization. Our findings suggest that dysregulation of PARIS may contribute to metabolic diseases, such as obesity, T2D, and NAFLD. Future investigations should dissect the transcriptional mechanisms by which PARIS modulates lipid metabolism genes and explore the potential therapeutic benefits of targeting PARIS in metabolic disorders.

Methods

Animals

The experimental procedures and reporting of this study were conducted in accordance with the ARRIVE guidelines. All animal experiments and protocols adhered to the Fundamental Guidelines for Proper Conduct of Animal Experiment and Related Activities, as stipulated by the Ministry of Education, Culture, Sports, Science and Technology of Japan. The experiments were approved by the Ethics Review Committee for Animal Experimentation at Tokyo University of Science (Approval Nos: Y20043, Y21043, Y22037). C57BL/6 mice were housed in a specific pathogen-free environment and had free access to the CRF-1 diet (Oriental Yeast, Tokyo, Japan) and water.

At 8 weeks of age, male mice were divided into two groups: the ND group was fed a control CRF-1 diet and the HFD group was fed High-Fat Diet 32 (CREA, Tokyo, Japan) for 14 weeks.

At 22 weeks of age, mice were euthanized and the following tissues were removed, diced, frozen in liquid nitrogen, and stored at −80 °C until use: epididymal WAT (eWAT), subcutaneous WAT (sWAT), kidneys, liver, lungs, and heart. Because of technical and ethical considerations, some experiments were conducted using a small sample size (n = 3). Despite this, all measurements showed consistent trends and met statistical significance thresholds. Larger cohort sizes will be considered for future validation studies. Euthanasia was performed via inhalation of isoflurane at an overdose concentration until respiratory arrest, followed by confirmation of death. This procedure adhered to institutional and national guidelines, and conformed to the American Veterinary Medical Association Guidelines for the Euthanasia of Animals (2020), minimizing animal suffering.

Humane endpoints were established based on observable clinical signs such as severe weight loss (> 20%), abnormal posture, reduced mobility, or lack of grooming. Mice exhibiting these signs were humanely euthanized to minimize suffering.

Generation of P7KO mice

Frozen sperm from a conditional *Znf746* (PARIS) floxed mouse line carrying loxP sites flanking exon 7 were obtained from the Korea Mouse Phenotyping Center at Seoul National University (Seoul, South Korea) and shipped to the Laboratory Animal Resource Center at the University of Tsukuba (Tsukuba, Japan), where in vitro fertilization was performed using C57BL/6 J oocytes. Fertilized one-cell embryos were electroporated with mRNA encoding Flp recombinase to excise the flippase recognition target-flanked selection cassette. The resulting embryos were transferred into pseudopregnant females, and $Znf746^{flox/flox}$ mice were established following genotypic confirmation. $Znf746^{flox/flox}$ mice were first crossed with CAG-Cre transgenic mice

(C57BL/6-Tg[CAG-cre]13Miya)[34] obtained from the RIKEN BioResource Research Center (Catalog no. RBRC09807; Tsukuba, Japan) to generate *Znf746*$^{flox/wt}$; CAG-Cre^{+} mice. These mice were then intercrossed to obtain *Znf746*$^{flox/flox}$; CAG-Cre^{+} mice, in which *Znf746* exon 7 is deleted in the germline. To eliminate the CAG-Cre transgene, *Znf746*$^{flox/flox}$; CAG-Cre^{+} mice were crossed with wild-type C57BL/6 mice to obtain Znf746$^{\Delta ex7/wt}$; Cre^{-} mice, followed by intercrossing to generate Znf746$^{\Delta ex7/\Delta ex7}$; Cre^{-} mice. These mice were designated as PARIS Δex7 or P7KO.

Schematic drawings of the gene targeting and breeding strategy are provided in Supplementary Figure S1A and C. Genotyping PCR was performed to confirm the presence of the floxed allele (Supplementary Fig. S1B), deletion of exon 7 (Supplementary Fig. S1D), and removal of CAG-Cre (Supplementary Fig. S1E). The primer sequences used for genotyping are listed in Supplementary Table 1. Sample sizes (n = 6–7 per group) were based on previous studies employing similar metabolic phenotyping under HFD conditions in C57BL/6 J mice. Group sizes were chosen to ensure adequate statistical power while adhering to ethical guidelines to minimize animal use.

CT

CT was performed as previously described using the LaTheta LCT-200 (Hitachi-Aloka, Tokyo, Japan), a third-generation CT scanner[35]. Briefly, mice were scanned at 50 kV and 0.5 mA with a resolution of 96 μm/pixel. Scanning conditions were optimized in pilot experiments and included a − 550 to − 140 Hounsfield unit density range, 240 μm slice thickness, and 1500 μm slice pitch.

Intraperitoneal GTT and ITT

GTTs and ITTs were performed on HFD-fed WT and P7KO mice at 19 and 20 weeks of age, respectively, following a 6 h fast. Mice were intraperitoneally injected with a 1.0 g/kg body weight dose of D-glucose (Wako, Osaka, Japan) for GTT, or a 40 μg/kg dose of insulin (Wako, Osaka, Japan) for ITT, followed by serial blood sampling from the tail vein at 0, 15, 30, 60, and 120 min post injection. Blood glucose levels were measured using the ACCU-CHECK® Aviva (Roche, Basel, Switzerland).

Measurement of triglycerides and total cholesterol in the liver

Total lipids were extracted from the liver using a modified Folch method. Briefly, approximately 50–100 mg of minced liver tissue was weighed into a 2.0 mL tube, followed by the addition of 500 μL of Solution I (chloroform:methanol = 2:1) and stainless-steel beads. The tissue was homogenized using a bead homogenizer (six cycles of 3,000 rpm for 10 s). The beads were removed and 600 μL of Solution I was added to the tube. Next, 275 μL of 1 M NaCl was added to the tube and vortexed. Samples were centrifuged at 2,100 × g for 10 min at 4 °C, the upper aqueous layer was removed, and the chloroform layer was transferred to a new 1.5 mL tube, avoiding the tissue layer. The chloroform layer was then dried at 37 °C for approximately 1 day. The dried sample was resuspended in an appropriate volume of Solution II (tert-butanol:methanol:Triton X-114 = 3:1:1). The final solution was stored at 4 °C for short use or at − 20 °C for long-term storage. Triglycerides and total cholesterol were measured using the LabAssay™ Triglyceride and LabAssay™ Cholesterol kits (WAKO, Osaka, Japan), in accordance with the manufacturer's protocols.

H&E staining

Formalin-fixed, paraffin-embedded tissue sections were deparaffinized and stained with H&E. Stained sections were visualized using a Bz- × 810 optical microscope (Keyence, Osaka, Japan).

Western blotting

Dissected tissues were lysed in lysis buffer (50 mM Tris–HCl pH 6.8, 2% sodium dodecyl sulfate [SDS], 3 M urea, 6% glycerol), sonicated, and boiled for 5 min. Protein concentrations of the soluble fraction were determined using the bicinchoninic acid protein assay (Thermo Fisher Scientific, Waltham, MA, USA) following the manufacturer's protocol, and standardized by the addition of lysis buffer. Protein samples were then mixed with 2-Mercaptoethanol and bromophenol blue to obtain final concentrations of 5 and 0.025%, respectively, and boiled for 5 min. Lysates containing 15 μg protein were subjected to SDS–polyacrylamide gel electrophoresis, and the separated proteins were transferred to nitrocellulose membranes. The membranes were blocked with 2.5% skimmed milk and 0.25% bovine serum albumin in Tris-buffered saline (50 mM Tris–HCl pH 7.4 and 150 mM NaCl) containing 0.1% Tween 20 for 60 min at room temperature, and then incubated with appropriate primary antibodies overnight at 4 °C. The membranes were then incubated with an appropriate secondary antibody for 60 min at room temperature. Finally, the membranes were incubated with ImmunoStar LD (Wako). Specific protein bands were visualized using ChemiDoc (Bio-Rad, Hercules, CA, USA), and the data were analyzed using Image Lab software. The antibodies used for this study are listed in Supplementary Table 2.

For all Western blot experiments in this study, membranes were cut prior to antibody hybridization in order to allow simultaneous probing with different antibodies. Original uncropped blot images, including membrane edges and all replicates, are provided in the Supplementary Information. For blots where high contrast limited the visibility of membrane edges (e.g., Figs. 4F, 5F, and Supplementary Fig. 3E), both high- and low-contrast versions obtained using Image Lab software (Bio-Rad, Hercules, CA, USA) are included in the Supplementary Information.

RT-PCR

RNA was extracted from tissues and cell pellets using ISOGENII (Nippon Gene, Tokyo, Japan). Purified RNA was reverse transcribed using ReverTra Ace® qPCR RT Master Mix (Toyobo, Osaka, Japan), and cDNAs were amplified with gene-specific primers using a CFX Connect™ Real-time System in Thunderbird SYBR qPCR mix

(Toyobo), in accordance with the manufacturer's protocols. Target gene expression data were normalized to *Rps18* expression. The sequences of the primers used for this study are listed in Supplementary Table 1.

Statistical analysis

Statistical analyses were performed using GraphPad Prism. Data were analyzed using Student's t-tests. Differences with a P value < 0.05 were considered to indicate statistical significance.

Data availability

All data generated or analyzed during this study are included in this published article and its supplementary information files. The complete raw datasets used to generate the main figures—including qPCR Ct values, Western blot intensity, and individual mouse phenotypic measurements—are provided in Supplementary Data 1. Additional datasets related to this study are available from the corresponding author upon reasonable request.

Received: 18 April 2025; Accepted: 11 September 2025
Published online: 15 October 2025

References

1. Sun, H. et al. IDF diabetes atlas: Global, regional and country-level diabetes prevalence estimates for 2021 and projections for 2045. *Diabetes Res. Clin. Pract.* **183**, 109119. https://doi.org/10.1016/j.diabres.2021.109119 (2022).
2. Daousi, C. et al. Prevalence of obesity in type 2 diabetes in secondary care: association with cardiovascular risk factors. *Postgrad. Med. J.* **82**, 280–284. https://doi.org/10.1136/pmj.2005.039032 (2006).
3. Knowler, W. C. et al. Reduction in the incidence of type 2 diabetes with lifestyle intervention or metformin. *N. Engl. J. Med.* **346**, 393–403. https://doi.org/10.1056/NEJMoa012512 (2002).
4. Khan, M. A. B. et al. Epidemiology of type 2 diabetes - global burden of disease and forecasted trends. *J. Epidemiol. Glob. Health* **10**, 107–111. https://doi.org/10.2991/jegh.k.191028.001 (2020).
5. Ahmad, E., Lim, S., Lamptey, R., Webb, D. R. & Davies, M. J. Type 2 diabetes. *Lancet* **400**, 1803–1820. https://doi.org/10.1016/s0140-6736(22)01655-5 (2022).
6. Jo, J. et al. Hypertrophy and/or hyperplasia: dynamics of adipose tissue growth. *PLoS Comput. Biol.* **5**, e1000324. https://doi.org/10.1371/journal.pcbi.1000324 (2009).
7. Horwitz, A. & Birk, R. Adipose Tissue hyperplasia and hypertrophy in common and syndromic obesity-the case of BBS obesity. *Nutrients* https://doi.org/10.3390/nu15153445 (2023).
8. Ye, R. Z., Richard, G., Gévry, N., Tchernof, A. & Carpentier, A. C. Fat cell size: Measurement methods, pathophysiological origins, and relationships with metabolic dysregulations. *Endocr. Rev.* **43**, 35–60. https://doi.org/10.1210/endrev/bnab018 (2022).
9. Müller, C. et al. Enhanced C/EBPβ function promotes hypertrophic versus hyperplastic fat tissue growth and prevents steatosis in response to high-fat diet feeding. *Elife* https://doi.org/10.7554/eLife.62625 (2022).
10. Ye, R. Z. et al. Adipocyte hypertrophy associates with in vivo postprandial fatty acid metabolism and adipose single-cell transcriptional dynamics. *iScience* **27**, 108692. https://doi.org/10.1016/j.isci.2023.108692 (2024).
11. Cannavino, J. & Gupta, R. K. Mesenchymal stromal cells as conductors of adipose tissue remodeling. *Genes Dev.* **37**, 781–800. https://doi.org/10.1101/gad.351069.123 (2023).
12. Gustafson, B. et al. Inflammation and impaired adipogenesis in hypertrophic obesity in man. *Am. J. Physiol. Endocrinol. Metab.* **297**, e999-e1003. https://doi.org/10.1152/ajpendo.00377.2009 (2009).
13. Hachiya, K. et al. Obesity-induced PARIS (ZNF746) accumulation in adipose progenitor cells leads to attenuated mitochondrial biogenesis and impaired adipogenesis. *Sci. Rep.* **13**, 22990. https://doi.org/10.1038/s41598-023-49996-0 (2023).
14. Rabby, M. G., Suzauddula, M., Hasan, M. S., Dewan, M. A. & Islam, M. N. In-silico identification and functional characterization of common genes associated with type 2 diabetes and hypertension. *Heliyon* **10**, e36546. https://doi.org/10.1016/j.heliyon.2024.e36546 (2024).
15. Yazar, V., Kang, S. U., Ha, S., Dawson, V. L. & Dawson, T. M. Integrative genome-wide analysis of dopaminergic neuron-specific PARIS expression in Drosophila dissects recognition of multiple PPAR-γ associated gene regulation. *Sci. Rep.* **11**, 21500. https://doi.org/10.1038/s41598-021-00858-7 (2021).
16. Shin, J. H. et al. PARIS (ZNF746) repression of PGC-1α contributes to neurodegeneration in Parkinson's disease. *Cell* **144**, 689–702. https://doi.org/10.1016/j.cell.2011.02.010 (2011).
17. LaPak, K. M. et al. Proximity proteomic analysis of the NRF family reveals the Parkinson's disease protein ZNF746/PARIS as a co-complexed repressor of NRF2. *Sci. Signal* **16**, eadi9018. https://doi.org/10.1126/scisignal.adi9018 (2023).
18. Cerezo, M. et al. The NHGRI-EBI GWAS catalog: standards for reusability, sustainability and diversity. *Nucleic Acids Res.* **53**, D998-d1005. https://doi.org/10.1093/nar/gkae1070 (2025).
19. Harrison, P. W. et al. Ensembl 2024. *Nucleic Acids Res.* **52**, D891-d899. https://doi.org/10.1093/nar/gkad1049 (2024).
20. Entrop, K., Wieske, S. & Rehm, M. Why Bax detection in >1400 publications might be flawed. *Cell Death Dis.* **15**, 880. https://doi.org/10.1038/s41419-024-07273-6 (2024).
21. Stevens, D. A. et al. Parkin loss leads to PARIS-dependent declines in mitochondrial mass and respiration. *Proc. Natl. Acad. Sci. USA* **112**, 11696–11701. https://doi.org/10.1073/pnas.1500624112 (2015).
22. Choy, L. & Derynck, R. Transforming growth factor-beta inhibits adipocyte differentiation by Smad3 interacting with CCAAT/enhancer-binding protein (C/EBP) and repressing C/EBP transactivation function. *J. Biol. Chem.* **278**, 9609–9619. https://doi.org/10.1074/jbc.M212259200 (2003).
23. Macotela, Y. et al. Intrinsic differences in adipocyte precursor cells from different white fat depots. *Diabetes* **61**, 1691–1699. https://doi.org/10.2337/db11-1753 (2012).
24. Lessard, J. et al. Low abdominal subcutaneous preadipocyte adipogenesis is associated with visceral obesity, visceral adipocyte hypertrophy, and a dysmetabolic state. *Adipocyte* **3**, 197–205. https://doi.org/10.4161/adip.29385 (2014).
25. Ibrahim, M. M. Subcutaneous and visceral adipose tissue: structural and functional differences. *Obes. Rev.* **11**, 11–18. https://doi.org/10.1111/j.1467-789X.2009.00623.x (2010).
26. Wang, X. et al. Depot-specific differences in fat mass expansion in WT and ob/ob mice. *Oncotarget* **8**, 46326–46336. https://doi.org/10.18632/oncotarget.17938 (2017).
27. Kobayashi, M., Deguchi, Y., Nozaki, Y. & Higami, Y. Contribution of PGC-1α to obesity- and caloric restriction-related physiological changes in white adipose tissue. *Int. J. Mol. Sci.* https://doi.org/10.3390/ijms22116025 (2021).
28. Jang, H. et al. Adipose tissue hyperplasia with enhanced adipocyte-derived stem cell activity in Tc1(C8orf4)-deleted mice. *Sci. Rep.* **6**, 35884. https://doi.org/10.1038/srep35884 (2016).
29. Ecco, G., Imbeault, M. & Trono, D. KRAB zinc finger proteins. *Development* **144**, 2719–2729. https://doi.org/10.1242/dev.132605 (2017).

30. Thomas, J. H. & Emerson, R. O. Evolution of C2H2-zinc finger genes revisited. *BMC Evol. Biol.* **9**, 51. https://doi.org/10.1186/1471-2148-9-51 (2009).
31. Hamilton, A. T. et al. Evolutionary expansion and divergence in the ZNF91 subfamily of primate-specific zinc finger genes. *Genome Res.* **16**, 584–594. https://doi.org/10.1101/gr.4843906 (2006).
32. Huntley, S. et al. A comprehensive catalog of human KRAB-associated zinc finger genes: insights into the evolutionary history of a large family of transcriptional repressors. *Genome Res.* **16**, 669–677. https://doi.org/10.1101/gr.4842106 (2006).
33. Nowick, K., Hamilton, A. T., Zhang, H. & Stubbs, L. Rapid sequence and expression divergence suggest selection for novel function in primate-specific KRAB-ZNF genes. *Mol. Biol. Evol.* **27**, 2606–2617. https://doi.org/10.1093/molbev/msq157 (2010).
34. Sakai, K. & Miyazaki, J. A transgenic mouse line that retains Cre recombinase activity in mature oocytes irrespective of the cre transgene transmission. *Biochem. Biophys. Res. Commun.* **237**, 318–324. https://doi.org/10.1006/bbrc.1997.7111 (1997).
35. Narita, T. et al. Differential response to caloric restriction of retroperitoneal, epididymal, and subcutaneous adipose tissue depots in rats. *Exp. Gerontol.* **104**, 127–137. https://doi.org/10.1016/j.exger.2018.01.016 (2018).

Acknowledgements

This work was supported by JST SPRING (Grant no. JPMJSP2151). We thank Michelle Kahmeyer-Gabbe, PhD, from Edanz (https://jp.edanz.com/ac) for editing a draft of this manuscript.

Author contributions

Yoshikazu Higami (Y.H.) supervised the study. Kazuki Hachiya (K.H.), Yuhei Mizunoe (Y.M.), Yuka Nozaki (Y.N.), and Masaki Kobayashi (M.K.) developed the study concept. K.H. and Y.M. wrote the main manuscript. Seiya Mizuno (S.M.) and Satoru Takahashi (S.T.) designed and generated the genetically modified mice. K.H., Joo-Joo Yang (J.J.Y.), Yuki Uchida (Y.U.), Hiroto Fukai (H.F.), and Tatsuhiro Esashi (T.E.) performed the experiments and data analysis. All authors reviewed the manuscript and agreed to its submission.

Funding

This work was supported by JST SPRING (Grant No. JPMJSP2151), the Japan Society for the Promotion of Science (JSPS KAKENHI Grant Nos. 25K14920 and 22K11889).

Declarations

Competing interests

The authors declare no competing interests.

Additional information

Supplementary Information The online version contains supplementary material available at https://doi.org/10.1038/s41598-025-19977-6.

Correspondence and requests for materials should be addressed to Y.H.